Izvestiya, Atmospheric and Oceanic Physics, Vol. 41, No. 6, 2005, pp. 726–740. Translated from Izvestiya AN. Fizika Atmosfery i Okeana, Vol. 41, No. 6, 2005, pp. 798–813.

Analysis of the CHAMP Experimental Data on Radio-Occultation Sounding of the Earth's Atmosphere

M. E. Gorbunov*, K. B. Lauritsen, A. Rodin***, M. Tomassini***, and L. Kornblueh******

** Oboukhov Institute of Atmospheric Physics, Russian Academy of Sciences, Pyzhevskii per. 3, Moscow, 119017 Russia*
*** Danish Meteorological Institute, Copenhagen DK-2100, Denmark*
**** German Weather Service, Offenbach D-63004, Germany*
***** Max Planck Institute for Meteorology, Hamburg D-20146, Germany*
e-mail: gorbunov@dkrz.de, andreas.rhodin@dwd.de
Received April 23, 2004; in final form, May 12, 2005

Abstract—A method of processing the radio-occultation data on the Earth's atmosphere obtained from the Challenging Minisatellite Payload (CHAMP) is described. The method includes (i) filtering noises and inferior data on the basis of analysis of local spatial spectra of the measured wave field, (ii) determining bending angles by the canonical transform method, (iii) evaluating errors in the resulting bending angles from analysis of local spectra of the transformed wave field, and (iv) evaluating errors in the retrieved temperature profiles. Examples of processing and analyzing the measurement data are presented.

1. INTRODUCTION

Satellite radio-occultation sounding is a promising method of studying the Earth's atmosphere for weather forecasting and for revealing climate changes [1]. The use of Global Positioning System (GPS) signals for radio-occultation sounding was proposed in [2]. A high frequency stability of GPS signals ensures the accuracy of determining atmospheric parameters required for dynamic weather forecasting. The first radio-occultation experiment based on GPS signals was conducted using the Microlab-1 satellite in 1995 [3, 4]. The data obtained with the Microlab-1 satellite during 1995–1997 have demonstrated high potentialities of the radio occultation method [5–7]. At the present time, the Microlab-1 satellite resources have been exhausted. In 2000, the Challenging Minisatellite Payload (CHAMP) [8] was launched, which performed 200 to 300 daily occultation events.

The principle of radio-occultation sounding lies in measuring and interpreting the amplitudes and phases of radio signals transmitted through the Earth's atmosphere. The source of the signals is a GPS satellite, and the receiver is located on a low-orbit satellite (an orbital altitude of about 700 km above the Earth's surface). The propagation of radio waves is controlled by the atmospheric refractive index, which is the given function of pressure, temperature, and humidity. From measured radio signals, the spatial distribution of the refractive index is retrieved. In polar regions, the contribution of humidity is small at all altitudes, and, in the tropics, it is small above 7–10 km. If the contribution of humidity to the refractive index can be neglected, the hydrostatic equation makes it possible to determine temperature and pressure profiles from a refractive-index profile. If the contribution of humidity is significant, it is necessary to use either additional data (such as prior humidity or temperature profiles from forecasts [4]) or schemes of direct variational assimilation [9–12]. Major data on radio-occultation sounding are presented in Section 2.

The wave fields measured in radio-occultation experiments are interpreted in two steps. First, the bending angles are calculated, and, after that, the inverse problem of determining the vertical profile of the refractive index from the refraction-angle profile is solved. This paper describes original algorithms for determining bending angles from wave fields.

The simplest approach to determining bending angles from measurements of the Doppler frequency is based on the geometric-optics approximation and the assumption of single-path propagation [13]. This approach is invalid in the troposphere, where the effects of multipath propagation and diffraction become important owing to a complex structure of the refractive-index field. The simplest method of determining bending angles in multipath regions is based on an analysis of local spatial spectra of the measured wave field in moving apertures [14–16]. The canonical transform method for reconstructing the ray structure of a wave field was proposed in [17]. This method uses Fourier integral operators, which allow the extension of the formalism of canonical transforms used in geometric optics to wave optics. A canonical transform is considered such that the projection of the ray manifold onto the new coordinate axis is single-valued. The corresponding Fourier integral operator transforms the wave

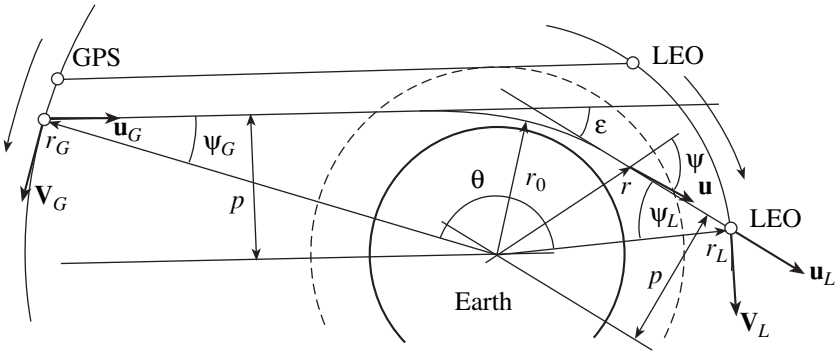

Fig. 1. Geometry of radio-occultation sounding.

field into a representation in which there is no multipath propagation. The canonical transform method yields a substantially higher accuracy of determining bending angles in comparison with analysis of local spatial spectra.

The canonical transform method was modified in [18], where the global-spectrum method was introduced. This method is based on the fact that the Fourier integral operator reduces to the Fourier transformation in the case of a circular geometry of radio setting (circular coplanar satellite orbits, a spherical shape of the Earth). An approximate operator was constructed in [18] to take into account departures of a real geometry of observations from the circular geometry. The authors of [19] introduced a new type of Fourier integral operators (the second type, as distinguished from the first type used previously [19]), which extends the global-spectrum method to an arbitrary geometry of radio setting. An exact solution for the phase function of such an integral operator was obtained in [20]. This solution is exact; however, the operator with such a phase function does not reduce to the Fourier transformation in a general case. This substantially reduces the efficiency of a numerical algorithm based on this operator.

Fourier integral operators of the second type are considered in Section 3. Equations for their amplitude and phase functions are derived, and the solutions of these equations are obtained. The relation of these operators to canonical transforms is considered. On the basis of the linearization of the canonical transform, we construct an approximation reducing the operator to the Fourier transformation for an arbitrary realistic geometry of observations.

Experimental data processing requires the filtering of noises and inferior data. It is also necessary to evaluate the errors in the refraction-angle profiles obtained and in the retrieved temperature profiles. These problems are considered in Section 4 and are solved by analyzing local spatial spectra of both the measured field and the wave field transformed into the representation of ray coordinates by using the Fourier integral operator. Although this method shows a rather low resolution in multipath regions, it has a wider range of applicability and is very suitable for data visualization. The width of the spectrum is a very convenient measure of measurement errors. Thus, analysis of local spectra represents a method additional to the methods based on global Fourier integral operators.

Examples of processing the data of CHAMP measurements are presented. We demonstrate the application of the aforementioned method to analysis of the data of measurements in the lower troposphere, where the errors in signal tracking increase substantially. The visualization of local spatial spectra clearly demonstrates the high quality of measurement data. Retrieved temperature profiles and the estimates of their errors are presented. Statistical comparison of the CHAMP data with the data of the German Weather Service is made.

2. INFORMATION ON RADIO-OCCULTATION SOUNDING

In the course of a radio-occultation experiment, the satellites move so that the radio ray connecting the transmitter and receiver descends into the atmosphere (Fig. 1). The signal amplitude and phase are measured. The experiment is conducted until the radio-shadow region is reached, where a weak signal cannot be measured. The transmitter is located on a GPS satellite, and the receiver is located on a low Earth orbiter (LEO). The measured wave field is $U(t) = C(t)A(t)\sin(ik\Psi(t) - i\omega t)$, where ω is the transmitter's frequency, $A(t)$ is the amplitude of the received signal, $\Psi(t)$ is the optical path of the beam between the transmitter and the receiver, and $C(t)$ is the modulation of the GPS signal by a pseudorandom code. Digital processing of the measured field $U(t)$ is used to demodulate the signal and to determine its complex amplitude $u(t) = A(t)\exp(ik\Psi t)$ [21–23]. The vacuum optical path $\Psi_0(t)$ calculated for a direct beam between the transmitter and the receiver is subtracted from the total optical path. The radio-occultation data contain the amplitude $A(t)$ and the atmospheric optical path $\Delta\Psi(t) = \Psi(t) - \Psi_0(t)$, as well as satellite orbital data.

Consideration for relativistic effects is important in calculating $\Psi_0(t)$ [13]. However, the relativistic factor

depends only on the magnitudes of satellite velocities and it is cancelled in the difference $\Psi(t) - \Psi_0(t)$ with a relative accuracy of $V^2/c^2 \approx 10^{-9}$. Consequently, if the atmospheric optical path was calculated correctly at the stage of data preprocessing, we can calculate the optical path $\Psi(t)$ as the sum of $\Delta\Psi(t)$ and the distance between the transmitter and the receiver by using nonrelativistic theory. The relative errors in the bending angles constitute 10^{-9}, which is three to four orders of magnitude smaller than the main measurement and calculation errors.

The derivative of the optical path $\dot{\Psi}$ is equal to $\mathbf{V}_L\mathbf{u}_L - \mathbf{V}_G\mathbf{u}_G$, where $\mathbf{V}_{L,G}$ are the satellite velocities and $\mathbf{u}_{L,G}$ are the unit vectors in the directions of the beam near the transmitter and receiver, respectively. (Hereafter, the index G denotes a GPS satellite and the index L denotes a LEO.) This expression will be represented as the sum of the contributions of the angular and radial components of the satellite velocities. From satellite orbital data, one can determine the distances $r_G(t)$ and $r_L(t)$ of the satellites from the Earth's center and the angular separation $\theta(t) = \theta_L(t) - \theta_G(t)$, where $\theta_G(t)$ and $\theta_L(t)$ are the angular coordinates of the satellites in the instantaneous vertical plane (Fig. 1). It can be written that [24]

$$\begin{aligned}\dot{\Psi} &= \dot{\theta}_L r_L \sin\psi_L - \dot{\theta}_G r_G \sin\psi_G \\ &\quad + \dot{r}_L \cos\psi_L + \dot{r}_G \cos\psi_G.\end{aligned} \tag{1}$$

Under the assumption of local spherical symmetry [25], the impact parameter (impact height) of the beam p is the same for the transmitter and receiver: $p = r_L\sin\psi_L = r_G\sin\psi_G$. This is a special case of Bouguer's formula (or the Snell law) for a spherically layered medium: $rn(r)\sin\psi = p$, where $n(r)$ is the vertical profile of the atmospheric refractive index. As a result, the derivative of the optical path of the beam can be written as follows [24]:

$$\dot{\Psi} = \eta(p, t) \equiv \dot{\theta}p + \frac{\dot{r}_L}{r_L}\sqrt{r_L^2 - p^2} + \frac{\dot{r}_G}{r_G}\sqrt{r_G^2 - p^2}. \tag{2}$$

Here, $\dot{\Psi}$ is the measured quantity and $\dot{\theta}$, $\dot{r}_{L,G}$ and $r_{G,L}$ are the known functions of time t; therefore, the right-hand side $\eta(p, t)$ will be the known function of p and t. Consequently, if the measurements of $\dot{\Psi}(t)$ are specified, one can solve Eq. (2) for $p(t)$. (Although the solution is not unique, it is easy to choose a unique solution that is physically meaningful.) The simplest way to solve Eq. (2) is numerical because its analytical solution is very cumbersome. The bending angle (bending) of the beam ε is determined by the simple geometrical relation

$$\varepsilon = \theta - \arccos\frac{p}{r_L} - \arccos\frac{p}{r_G}. \tag{3}$$

The bending angle $\varepsilon(t)$ is calculated on the basis of (3) from the known function $p(t)$ and orbital data on $r_G(t)$, $r_L(t)$, and $\theta(t)$. The functions $p(t)$ and $\varepsilon(t)$ specify the profile of the bending angle $\varepsilon(p)$ in a parametric form. The above consideration is based substantially on the assumption that only one beam is observed at each moment t. In the case of the interference of many beams, the calculation of the profiles of the bending angle from the derivative of the optical path leads to unlikely strongly oscillating profiles of the bending angle [17]. Methods for determining the bending angles in multipath regions will be discussed in Section 3.

With the aid of the Abelian transformation, it is possible to find the profile of the index of refraction from the profile of the bending angle [26]:

$$n(x) = \frac{1}{\pi}\exp\left(\int_x^\infty \frac{\varepsilon(p)dp}{\sqrt{p^2 - x^2}}\right), \tag{4}$$

where $x(r) = rn(r)$ is the refraction radius. The retrieved profile $n(x)$ and the dependence $r(x) = x/n(x)$ specify the profile $n(r)$ in a parametric form.

This study disregards the retrieval of atmospheric humidity. If the effect of humidity is neglected, the refractive index will be [24]

$$n = 1 + C\frac{P}{T} = 1 + CR\rho, \tag{5}$$

where P is the pressure, T is the temperature, R is the gas constant of dry air, ρ is the density, and $C = 77.6 \times 10^{-6}$ K/hPa. With consideration for the equations of state and hydrostatics, it is possible to obtain the temperature from the retrieved profile of the refractive index [24]:

$$T(z) = \frac{\int_z^\infty g(z')\rho(z')dz'}{R\rho(z)} = \frac{\int_z^\infty g(z')[n(z') - 1]dz'}{R[n(z) - 1]}, \tag{6}$$

where $z = r - r_E$ is the height above the Earth's surface and $g(z)$ is the vertical profile of the acceleration of gravity.

3. RECONSTRUCTION OF THE RAY PATTERN OF WAVE FIELDS

For a complicated profile of the refractive index $n(r)$, the corresponding profile of the bending angle $\varepsilon(p)$ will be a nonmonotonic function. This will lead to the multipath propagation of a radio signal [14]. To see this, we will consider geometrical relation (3). It will be an equation for the impact parameters of the rays connecting the source to the receiver if the profile $\varepsilon = \varepsilon(p)$ is specified, and the relative position of the transmitter and receiver, which is determined by the parameters r_L, r_G, and θ, is fixed. Let us denote the right-hand side of (3) by $\varepsilon_G(p)$. We define the distances from the transmit-

ter and receiver to the Earth's limb, $D_{G,L} = \sqrt{r_{G,L}^2 - p^2}$, and the reduced observation distance $D = (D_L^{-1} + D_G^{-1})^{-1}$. Then, we may write

$$\frac{d\varepsilon_G(p)}{dp} = \frac{1}{D} > 0. \quad (7)$$

Thus, $\varepsilon_G(p)$ is a monotonically increasing function of the impact parameter. For a smooth exponential model of the atmosphere, $\varepsilon(p)$ decreases monotonically ($d\varepsilon(p)/dp < 0$) and the dependences $\varepsilon(p)$ and $\varepsilon_G(p)$ have no more than one intersection point for each position of the satellites. In this case, multipath propagation does not occur. However, if the dependence $\varepsilon(p)$ is nonmonotonic and such values of p exist at which $d\varepsilon(p)/dp > D^{-1}$, then there are observation points at which multiple rays arrive. It follows that a nonmonotonic profile $\varepsilon(p)$ will necessarily result in multipath propagation if the observation distance is sufficiently large.

The wave field in the region of multipath propagation can be approximated by the sum of the fields corresponding to different interfering rays:

$$u(t) = \sum_j u_j(t) = \sum_j A_j(t)\exp(ik\Psi_j(t)), \quad (8)$$

where the index j numbers the rays that interfere at the moment t and have the impact parameters $p_j(t)$. For the functions $p_j(t)$ and $\dot{\Psi}_j(t)$, relation (2) will be true. However, the decomposition of the total measured field $u(t)$ into the components $u_j(t)$ and the number of interfering rays are not known in advance; therefore, Eq. (2) cannot be used to determine the impact parameters immediately. It is also clear that the derivative of the eikonal $\dot{\Psi}(t)$ of the total field $u(t)$ cannot be substituted into (2) for a multipath region.

The simplest way to separate interfering rays is based on analysis of local spatial spectra. This approach was used previously for processing the data of sounding planetary atmospheres [27]. As applied to the Earth's atmosphere, it was modified through the use of a synthesized focused aperture [14–16, 28, 29]. In the context of this approach, spectral analysis of the wave field $u(t)$ is carried out with moving apertures:

$$\nu(t,\eta) = \int_{t-T/2}^{t+T/2} \frac{u(\tau)\cos\dfrac{\pi(\tau-t)}{T}}{A_m(\tau)\exp[ik(\Psi_m(\tau) - \dot{\Psi}_m(t)\tau)]} \times \exp(-ik\eta\tau)d\tau, \quad (9)$$

where $A_m(t)\exp(ik\Psi_m(t))$ is the reference signal determined for a smooth model of the refractive index and T is the aperture value. The use of the reference signal is important because it adjusts the curvature of the wave front, thus focusing the synthesized aperture [15, 28]. The peaks of the spectrum $|\nu(t,\eta)|$ for each t will reveal physical rays interfering at a given observation point. The impact parameter p and the bending angle ε can be expressed as functions $p(t,\eta)$ and $\varepsilon(t,\eta)$ from Eqs. (2) and (3). As a result, the amplitude of a local spatial spectrum can be obtained in a parametric form as a function of $|\nu(p,\varepsilon)|$. There is a limitation on the resolution of this method; however, it is very convenient for visualizing and diagnosing experimental data [30].

The canonical transform method will be used to determine the ray pattern of the wave field [17, 19]. This method lies in the following. There are measurements of the wave field $u(y) = A(y)\exp(ik\Psi(y))$ along the orbit of a satellite parameterized by an arbitrary coordinate y (in particular, $y = t$). It is necessary to determine the ray pattern of this field, i.e., ray directions at each point. In the context of the Hamilton formulation of geometrical optics, rays are described by the canonical Hamiltonian system of equations for the coordinate y and momentum η [31]. The momentum is equal to the derivative of the eikonal of the field $\partial\Psi/\partial y$ if there is only one ray at a given point y [31]. If multiple rays are present, their momenta η_j are determined on the basis of formula (8) as $\partial\Psi_j/\partial y$. Multiple rays appear in the case where the projection of the ray manifold onto the y axis is not unique [32]. The formula $\eta = \partial\Psi/\partial y$ is inapplicable in this case. A canonical transform of the coordinate and momentum in the phase space makes it possible to choose the new coordinate z and momentum ξ such that the projection of the ray manifold onto the new coordinate axis becomes unique [17]. The corresponding transformation of the wave field is implemented by the Fourier integral operator $\hat{\Phi}$. The momentum in the new representation $\hat{\Phi}u(z) = A'(z)\exp(ik\Psi'(z))$ can be determined from the transformed field $\xi(z) = \partial\Psi'/\partial z$.

The author of paper [17] used a Fourier integral operator, which was further referred to as the operator of the first type [19]. This operator was applied in combination with the operation of reverse propagation (wave-front reversal). For the generalization of the global-spectrum method [18], Fourier integral operators of the second type were introduced in [19]. These operators are applied immediately to the measured field $u(t)$ without preliminary reverse propagation, which leads to a higher numerical efficiency.

The Fourier integral operator of the second type has the form

$$\hat{\Phi}_2 u(z) = \sqrt{\frac{-ik}{2\pi}}\int a_2(z,t)\exp(ikS_2(z,t))u(t)dt. \quad (10)$$

The functions $a_2(z,t)$ and $S_2(z,t)$ are referred to as the amplitude and phase functions of the operator, respectively. Let us consider the relationship between this operator and canonical transforms. For this purpose, we will use the method of stationary phase. To simplify the notation, we will consider the field $u(t)$, meaning that an

individual component $u_j(t)$ can be considered when necessary. The point of stationary phase $t_s(z)$ of the integral in (10) is determined by the equation

$$\frac{\partial S_2(z,t)}{\partial t} = -\frac{d\Psi(t)}{dt} \equiv -\eta(t). \tag{11}$$

Let $\hat{\Phi}_2 u(z) = A'(z)\exp(ik\Psi'(z))$. The eikonal Ψ' of the transformed field $\hat{\Phi}_2 u(z)$ is

$$\Psi'(z) = S_2(z, t_s(z)) + \Psi(t_s(z)) + \frac{\gamma}{k}, \tag{12}$$

where $\gamma = \pm\pi/2$. The term γ/k vanishes asymptotically for large values of k, thus being unimportant for our analysis. Let us find the derivative of the eikonal, i.e., the momentum $\xi(z)$ of the transformed field, with consideration for Eq. (11):

$$\xi(z) \equiv \frac{d\Psi'(z)}{dz} = \frac{dt_s}{dz}\left(\frac{\partial S_2(z,t)}{\partial t} + \frac{d\Psi(t)}{dt}\right)\Bigg|_{t=t_s(z)} + \frac{\partial S_2(z,t)}{\partial z}\Bigg|_{t=t_s(z)} = \frac{\partial S_2(z,t_2(z))}{\partial z}. \tag{13}$$

The equation for the total differential of the phase function follows from Eqs. (11) and (13):

$$dS_2 = \xi dz - \eta dt. \tag{14}$$

The quantity ηdt is a truncated form of the action in the old representation. Similarly, ξdz is a truncated form of the action in terms of the transformed coordinate z. Since the difference $\xi dz - \eta dt$ is equal to the total differential dS_2, the transform $(t, \eta) \longrightarrow (x, \xi)$ is canonical [33]. A detailed analysis of the relationship between Fourier integral operators and canonical transforms was made in [34].

The amplitude function is determined from the condition of energy conservation

$$\left|\hat{\Phi}_2 u(z)\right|^2 dz = |u(t_s(z))|^2 \mu dt_s(z), \tag{15}$$

where $\mu = \mu(z, t)$ is the density of measure, which will be defined below. Using the conventional expression obtained for the amplitude by the method of stationary phase, we obtain

$$\left|\frac{|a_2(z,t)A(t)|^2}{-\frac{\partial^2 S_2(z,t)}{\partial t^2} - \frac{d^2\Psi(t)}{dt^2}}\right|_{t=t_s(z)} dz = A^2(t_s(z))|\mu dt_s(z)|. \tag{16}$$

It follows that the amplitude function can be written as

$$|a_2(z, t_s(z))|^2 = \left|-\frac{\partial^2 S_2(z,t)}{\partial t^2} - \frac{d^2\Psi(t)}{dt^2}\right|_{t=t_s(z)} \left|\mu \frac{dt_s(z)}{dz}\right|. \tag{17}$$

Differentiating the equation for the point of stationary phase (11) with respect to z, we obtain the following equation:

$$\left(\frac{\partial^2 S_2(z,t)}{\partial t^2} + \frac{d^2\Psi(t)}{dt^2}\right)\Bigg|_{t=t_s(z)} \frac{dt_s(z)}{dz} = -\frac{\partial^2 S_2(z,t)}{\partial z \partial t}\Bigg|_{t=t_s(z)}. \tag{18}$$

Therefore, the final expression for the amplitude function can be written as

$$a_2(z,t) = \sqrt{\left|\mu \frac{\partial^2 S_2(z,t)}{\partial z \partial t}\right|}. \tag{19}$$

Now, we will use the apparatus of Fourier integral operators to reconstruct the ray pattern of the measured wave field $u(t)$. Several rays with different impact parameters p can interfere at each moment t. The impact parameters of different rays in a spherically symmetrical layered medium always differ from one another. This result follows from the fact that the impact parameters of the rays produced by the transmitter are $p = r_G \sin\psi_G$. Since different rays have different directions ψ_G, these rays will have different impact parameters. Since the impact parameter of a ray is identical for the transmitter and receiver, all the rays received during the radio-occultation experiment will have different impact parameters.

Let us consider a ray manifold in the phase space with the coordinate t and momentum η. Multipath propagation occurs if the projection of the ray manifold onto the t axis is not unique. If we consider the new coordinate $z = p$, as is shown above, the projection of the ray manifold onto the p axis will be unique. Therefore, we will use the canonical transformation $(t, \eta) \longrightarrow (p, \xi)$, where the new momentum ξ will be determined from the canonicity condition.

Since the Fourier integral operator is bound to conserve energy, we start with the determination of the density of measure μ. Let the power of the transmitter be P. We require that the following equality be satisfied:

$$\frac{P}{2\pi} dp = A^2 \mu dt. \tag{20}$$

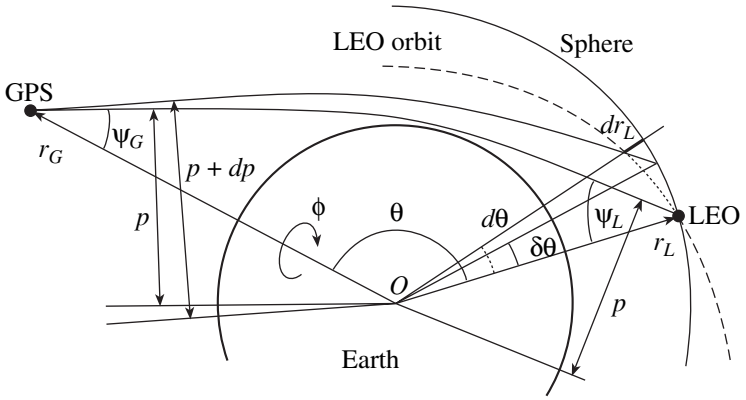

Fig. 2. Geometry of the ray tube for determining the amplitude of a radio-occultation signal.

The energy radiated within an infinitely small cone by a transmitter with an omnidirectional antenna is given by the expression [35]

$$dE_T = \frac{P}{4\pi} d\psi_G \sin\psi_G d\phi, \tag{21}$$

where P is the total power of radiation. The impact parameter p is equal to $r_G \sin\psi_G$. It follows that $dp = r_G \cos\psi_G d\psi_G = \sqrt{r_G^2 - p^2}\, d\psi_G$. Therefore, the following expression is obtained for the impact-parameter distribution of energy:

$$dE_T = \frac{P}{4\pi} \frac{1}{\sqrt{r_G^2 - p^2}} \frac{p}{r_G} d\phi dp. \tag{22}$$

Let us consider a receiving aperture in the form of an infinitely small element of a sphere centered at the Earth's center (Fig. 2). The received energy dE_R is equal to $A^2 \cos\psi_L dS$, where A is the refraction amplitude, ψ_L is the angle between the ray tube and the normal to the receiving aperture, and dS is the area of the aperture [35]:

$$\begin{aligned} dE_R &= \frac{1}{2} A^2 \cos\psi_L r_L r_L \sin\theta d\phi \delta\theta \\ &= \frac{1}{2} A^2 \sqrt{r_L^2 - p_L^2} r_L \sin\theta d\phi \delta\theta. \end{aligned} \tag{23}$$

The symbol δ is used to denote the partial differential calculated along the sphere at fixed r_L and r_G. Equating the transmitted and received energies, we obtain the following expression for the amplitude:

$$\begin{aligned} A^2 &= \frac{P}{2\pi} \frac{1}{\sqrt{r_L^2 - p^2}\sqrt{r_G^2 - p^2}} \\ &\times \frac{p}{r_G r_L \sin\theta} \frac{dp}{\delta\theta} \equiv \frac{P}{2\pi} \frac{dp}{\mu dt}. \end{aligned} \tag{24}$$

The size of a virtual receiving aperture $\delta\theta$ may be written as

$$\begin{aligned} \delta\theta &= d\theta - \left(\frac{\partial\theta}{\partial r_G}\right)_p dr_G - \left(\frac{\partial\theta}{\partial r_L}\right)_p dr_L \\ &= d\theta - \frac{dr_G}{r_G} \frac{p}{\sqrt{r_G^2 - p^2}} - \frac{dr_L}{r_L} \frac{p}{\sqrt{r_L^2 - p^2}}. \end{aligned} \tag{25}$$

From here, we obtain the following expression for the measure (under the assumption of spherical symmetry):

$$\begin{aligned} \mu &= \sqrt{r_L^2 - p^2}\sqrt{r_G^2 - p^2} \frac{r_L r_G}{p} \sin\theta \\ &\times \left(\dot\theta - \frac{\dot r_G}{r_G} \frac{p}{\sqrt{r_G^2 - p^2}} - \frac{\dot r_L}{r_L} \frac{p}{\sqrt{r_L^2 - p^2}} \right). \end{aligned} \tag{26}$$

With the use of Eqs. (2) and (14), we find the phase function [20, 34]

$$\begin{aligned} S_2(p,t) &= -\int \eta(p,t) dt = -\int \left(p d\theta + \frac{dr_G}{r_G} \sqrt{r_G^2 - p^2} \right. \\ &\left. + \frac{dr_L}{r_L} \sqrt{r_L^2 - p^2} \right) = -p\theta - \sqrt{r_G^2 - p^2} \\ &+ p \arccos\frac{p}{r_G} - \sqrt{r_L^2 - p^2} + p \arccos\frac{p}{r_L}. \end{aligned} \tag{27}$$

This expression is determined to within an arbitrary function $F(p)$, which will be assumed to be zero for convenience. The point of the path at which the ray with a given impact parameter p is observed will be denoted by $t_s(p)$. On the basis of formula (14), the derivative of the eikonal of the transformed field $\hat\Phi_2 u(p)$, or the new momentum ξ, is calculated as follows [20, 34]:

$$\xi(p) = \left.\frac{\partial S_2(p,t)}{\partial p}\right|_{t=t_s(p)} = -\theta + \arccos\frac{p}{r_G} + \arccos\frac{p}{r_L} = -\varepsilon(p). \quad (28)$$

Thus, to calculate the profile of the bending angle, the measured wave field is transformed using an operator of the second type. The transformed field is equal to $\hat{\Phi}_2 u(p) = A'(p)\exp(ik\Psi'(p))$. The derivative of its eikonal $\Psi'(p)$ taken with a negative sign is equal to the bending angle $\varepsilon(p)$. The phase function is defined to within an arbitrary function $F(p)$ and can be redefined as $S_2'(p,t) = S_2(p,t) + F(p)$. In this case, the momentum is $\xi' = \xi + dE(p)/dp$. This result corresponds to the multiplication of $\hat{\Phi}_2 u(p)$ by $\exp(ikF(p))$. The bending angle will be $\varepsilon(p) = -\xi' + dF(p)/dp$. Thus, the new momentum is determined to within an arbitrary function of the impact parameter. The choice of this function is unimportant.

In view of determining the amplitude function $a_2(p,t)$ from formulas (15) and (20), the amplitude of the transformed field $|\hat{\Phi}_2 u(p)|$ is close to a θ-function and is approximately constant in the illuminated region and decreases abruptly to small values in the shadow region [30].

For a circular geometry (r_G = const, r_L = const), the phase function depends linearly on θ and the dependence on θ in the amplitude function is factorable:

$$\hat{\Phi}_2 u(p) = \sqrt{\frac{-ik}{2\pi}}\exp\left[ik\left(-\sqrt{r_G^2-p^2} + p\arccos\frac{p}{r_G} - \sqrt{r_L^2-p^2} + p\arccos\frac{p}{r_G}\right)\right] \times\left(\sqrt{r_L^2-p^2}\sqrt{r_G^2-p^2}\frac{r_L r_G}{p}\right)^{1/2} \times\int\exp(-ikp\theta(t))u(t)\sqrt{\sin(\theta(t))}\dot{\theta}(t)dt. \quad (29)$$

As a result, the operator is reduced to a combination of the Fourier transformation of $u(t(\theta))\sqrt{\sin\theta}$ with respect to the variable θ and multiplication by the known function of p. We will describe the approximation that reduces this operator to the Fourier transformation for an arbitrary geometry of observations.

From Eq. (2), the impact parameter p can be expressed as a function $p(t, \eta)$. Instead of the exact impact parameter, we introduce its approximate value $\tilde{p}$

$$\tilde{p}(t,\eta) = p_0(t) + \frac{\partial p_0}{\partial\eta}(\eta - \eta_0(t)) = f(t) + \frac{\partial p_0}{\partial\eta}\eta, \quad (30)$$

$$f(t) = p_0(t) - \left.\frac{\partial p_0}{\partial\eta}\right|_{\eta=\eta_0(t)}\eta_0(t) = p_0 - \left(\dot{\theta} - \frac{\dot{r}_G}{r_G}\frac{p_0}{\sqrt{r_G^2-p_0^2}} - \frac{\dot{r}_L}{r_L}\frac{p_0}{\sqrt{r_L^2-p_0^2}}\right)^{-1}\eta_0, \quad (31)$$

where $\eta_0(t)$ is a smooth model of the derivative of the optical path and $p_0(t) = p(t, \eta_0(t))$. The model $\eta_0(t)$ can be obtained by differentiating the measured optical path with a strong smoothing. The error of this approximation of the impact parameter turns out to be about 1 m for a typical geometry of observations. Let us define a new parameter of the path $Y = Y(t)$ and the corresponding momentum σ as follows:

$$dY = \left(\frac{\partial p_0}{\partial\eta}\right)^{-1}dt = \frac{\partial\eta}{\partial p_0}dt, \quad (32)$$

$$\sigma = \frac{\partial p_0}{\partial\eta}\eta. \quad (33)$$

For brevity, we will use the notation $u(Y)$ instead of $u(t(Y))$. To switch to the representation of an approximate impact parameter, we introduce a linear canonical transform:

$$\tilde{p} = f(Y) + \sigma, \quad (34)$$

$$\xi = -Y. \quad (35)$$

Its generating function is determined from Eq. (14):

$$dS_2 = \xi d\tilde{p} - \eta dY = -Yd\tilde{p} - (\tilde{p} - f(Y))dY, \quad (36)$$

$$S_2(\tilde{p}, Y) = -\tilde{p}Y + \int_0^Y f(Y')dY'. \quad (37)$$

For dY, we have the following expression:

$$dY = d\theta - \frac{dr_G}{r_G}\frac{p_0}{\sqrt{r_G^2-p_0^2}} - \frac{dr_L}{r_L}\frac{p_0}{\sqrt{r_L^2-p_0^2}} \approx \delta\theta. \quad (38)$$

We can approximately write that $\delta\theta/dY \approx 1$. Since $|\partial^2 S_2/\partial\tilde{p}\,\partial Y| = 1$, the amplitude function is equal to $\sqrt{\mu}$:

$$a_2(\tilde{p}, Y) = \left(\sqrt{r_L^2-\tilde{p}^2}\sqrt{r_G^2-\tilde{p}^2}\frac{r_L r_G\sin\theta}{\tilde{p}}\right)^{1/2}. \quad (39)$$

The amplitude function $a^2(\tilde{p}, Y)$ in the operator $\hat{\Phi}_2$ can be replaced by $a_2(\tilde{p}, Y_s(\tilde{p}))$ and factored outside the integral sign. The resulting operator will be the composition of the multiplication of the field by the reference signal, Fourier transformation, and multiplication by the amplitude function:

$$\hat{\Phi}_2 u(\tilde{p}) = \sqrt{\frac{-ik}{2\pi}} a_2(\tilde{p}, Y_s(\tilde{p})) \times \int \exp(-ik\tilde{p}Y) \exp\left(ik \int_0^Y f(Y')dY' \right) u(Y)dY. \quad (40)$$

The function $Y_s(\tilde{p})$ is equal to $-\xi$, where the momentum ξ is equal to the derivative of the eikonal of the transformed field. In order to find the eikonal, it is possible first to substitute 1 for $a_2(\tilde{p}, Y_s(\tilde{p}))$ in (40), then to calculate the momentum ξ and to multiply the transformed wave function by $a_2(\tilde{p}, Y_s(\tilde{p}))$. The bending angle ε as a function of p and Y is determined by relation (3) and orbital data on $r_G(t(Y))$, $r_L(t(Y))$, and $\theta(t(Y))$. Substituting $Y = Y_s(p)$, we obtain the profile of the bending angle $\varepsilon(p)$:

$$\varepsilon(p) = \theta(t(Y_s(p))) - \arccos\frac{p}{r_L(t(Y_s(p)))} - \arccos\frac{p}{r_G(t(Y_s(p)))}. \quad (41)$$

4. ANALYSIS OF THE CHAMP DATA

Let us show how the method developed above is employed to analyze experimental data obtained from the CHAMP satellite. The measurement of signals in multipath regions, where the amplitude and phase of a signal are subject to strong fluctuations, is a complex engineering problem. In such conditions, the receiver often loses the signal or introduces significant errors in measurements [21, 22]. The quality of the CHAMP data for the troposphere (at heights below 10 km) is low [23, 36, 37]. The quality of a signal in channel L2 turns out to be especially low. Therefore, noise filtering is required.

The measurement data include satellite orbital data and the amplitudes $A_{1,2}(t_i)$ and atmospheric optical paths $\Delta\Psi_{1,2}(t_i)$ for two GPS channels (L1 at 1.57542 GHz and L2 at 1.22760 GHz) with a sampling rate of 50 Hz ($t_i = t_0 + 0.02i$ s). The total optical paths are calculated as $\Psi_{1,2}(t_i) = \Psi_0(t_i) + \Delta\Psi_{1,2}(t_i)$, where $\Psi_0(t_i)$ is the distance from the transmitter to the receiver. The velocity of the ray's vertical descent into the atmosphere is about 2 km/s under the conditions of weak refraction at heights above 10 km. This corresponds to a resolution of about 40 m. Owing to strong regular refraction, the velocity of the ray's descent is decreased in the troposphere and has an average value of 0.2 km/s near the Earth's surface.

Data processing consists of the following stages.

(1) Preprocessing. At this stage, terminal fragments of the data measured in the lower troposphere, where the signal-tracking errors are very large, are rejected. The data in channel L2 are also corrected because the signal-tracking errors in channel L2 are substantially greater than those in channel L1, a result which is due to the use of different algorithms of pseudorandom coding of signals in these two channels.

(2) Determination of the bending angles by using the method of Fourier integral operators developed in Section 3.

(3) Evaluation of the errors in the bending angles on the basis of analysis of the local spectra of the transformed wave field $\hat{\Phi}_2 u_1(p)$.

(4) Inversion of the bending angles and evaluation of the errors in temperature retrieval on the basis of the previously obtained errors in the bending angle.

4.1. Preprocessing of Measurement Data

At the first stage of data processing, a coarse estimate is made for the profile of the bending angle on the basis of formulas (2) and (3), where $\dot{\Psi}$ is calculated with a strong smoothing (with a vertical scale of about 2 km). The data starting at the time when the bending angle reaches 0.02 rad are rejected. Statistical analysis shows that such data are practically unsuitable for further processing.

Next, the local spatial spectra $\nu_{1,2}(t, \eta)$ of the signals $u_{1,2}(t) = A_{1,2}(t)\exp[ik_{1,2}\Psi_{1,2}(t)]$ are analyzed. An example of the spectra is shown in Figs. 3a and 3b. The spectra are recalculated to the coordinates ε, p with the use of the functions $\varepsilon(t, \eta)$ and $p(t, \eta)$ and are shown in pseudocolor. Instead of the impact parameter of a ray p, we use the impact height of the ray above the Earth's limb $p - r_E$, where r_E is the radius of local curvature of the geoid in the plane of radio setting. The ray tangent to the Earth has a typical impact height of $r_E(n(r_E) - 1) \simeq 2$ km because a typical value of the refractive index n at the Earth's surface is $1 + 3 \times 10^{-4}$ and $r_E \simeq 6370$ km. In channel L1, the spectra visualize the profile of the bending angle especially well for impact heights greater than 6.5 km. In channel L2, the situation is quite different. After the impact height of the ray reaches 6.5 km and the bending angle reaches 0.011 rad, the spectra exhibit a very rapid increase in the bending angle, which also leads to heavily overstated impact heights of rays because, for a fixed observation point, rays with a larger bending angle arrive from a larger height. This implies that the signal in channel L2 was lost and this portion of measurement data is completely erroneous and unsuitable for processing. A quality estimator for L2 signals is formed to reject such data and to filter noise. The mean of the impact parameter and its spectral width are calculated from the spectra:

$$\bar{p}_{1,2}(t) = \frac{\int |\nu_{1,2}(t, \eta)|^2 p(t, \eta)d\eta}{\int |\nu_{1,2}(t, \eta)|^2 d\eta}, \quad (42)$$

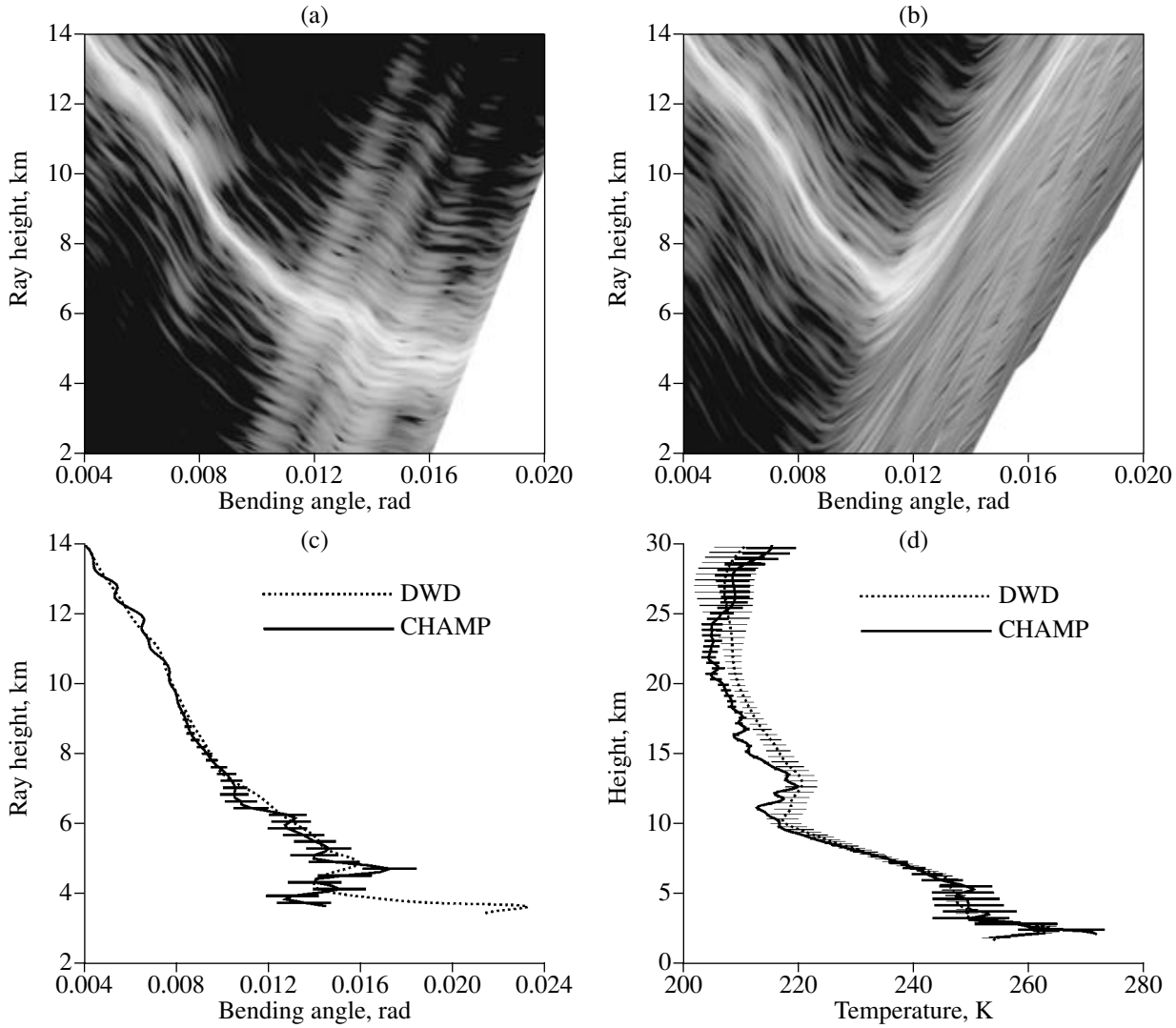

Fig. 3. Occultation event 0004, Jan. 18, 2004; UT = 00:24; 50.4° N, 116.1° W: (a) local spatial spectra for channel L1, (b) the same for channel L2, (c) bending angles calculated for the fields of DWD analyses and from the CHAMP data, and (d) temperature from the data of DWD analyses and CHAMP data.

$$\delta p_{1,2}(t) = \left(\frac{\int |\nu_{1,2}(t,\eta)|^2 (p(t,\eta) - \bar{p}_{1,2}(t))^2 d\eta}{\int |\nu_{1,2}(t,\eta)|^2 d\eta} \right)^{1/2}. \quad (43)$$

An empirical estimator is assumed to be

$$W(t) = 1 - \exp\left[-\frac{(\bar{p}_2(t) - \bar{p}_1(t))^2 + \delta p_2^2(t)}{\Delta p^2} \right], \quad (44)$$

where the parameter Δp equals 0.2 km. This estimator assesses the deterioration of the quality of data in channel L2. The indicators of data-quality deterioration are a large width of the spectrum $\delta p_2(t)$ and a large difference $\bar{p}_2(t) - \bar{p}_1(t)$ between the impact parameters in channels L1 and L2.

The smoothed phase paths are calculated from the profiles of the smoothed impact parameter:

$$\bar{\Psi}_{1,2}(t) = \int_{t_0}^{t} \eta(\bar{p}_{1,2}(t'), t') dt'. \quad (45)$$

The smoothed difference of ionospheric optical paths is calculated as $\Delta\bar{\Psi}(t) = \bar{\Psi}_2(t) - \bar{\Psi}_1(t)$ in the time interval when $W(t) < 0.7$. In the troposphere, where the quality of L2 signals is usually very low ($W(t) > 0.7$), the quantity $\Delta\bar{\Psi}(t)$ is extrapolated linearly. For this purpose, the linear regression of $\Delta\bar{\Psi}(t)$ is constructed between the time when the ray reaches a height of 30 km and the time when $W(t)$ attains a value of 0.7.

Let us denote the operation of calculating finite differences for the grid function by the symbol D_i: $D_iF = F(t_{i+1}) - F(t_i)$. The corrected optical path $\Psi_2^{\text{cor}}(t)$ and amplitude $A_2^{\text{cor}}(t)$ for channel L2 are defined as a linear combination of the L1 and L2 data with the weight determined by the estimator $W(t)$:

$$D_i\Psi_2^{\text{cor}} = D_i\Psi_2(1 - W(t_i)) + (D_i\Psi_1 + D_i\Delta\overline{\Psi})W(t_i), \quad (46)$$

$$\Psi_2^{\text{cor}}(t_i) = \sum_{j=1}^{i-1} D_j\Psi_2^{\text{cor}}, \quad (47)$$

$$A_2^{\text{cor}}(t_i) = A_2(t_i)(1 - W(t_i)). \quad (48)$$

The combination defined in terms of finite differences makes it possible to avoid the influence of the arbitrary constants $\Psi_{1,2}^0$ appearing in the definitions of the optical paths in channels L1 and L2. If a combination of the optical paths themselves is taken, the linear combination of two constants $\Psi_2^0(1 - W(t_i)) + \Psi_1^0(t_i)$ will no longer be a constant, thus leading to significant errors in calculating the bending angle.

4.2. Determination of the Bending Angles

The wave fields $u_1(t)$ and $u_2^{\text{cor}}(t)$ are transformed using the Fourier integral operator $\hat{\Phi}_2$ determined by formulas (37), (39), and (40). The bending angles $\varepsilon_{1,2}(p)$ are calculated by formula (41). The boundary of the geometrical-optics shadow p_1 is determined from the peak of the correlation between the amplitude $|\hat{\Phi}_2 u_1(p)|$ and the θ-function. For the data in channel L2, the peak p_2 of the correlation between the amplitude $|\hat{\Phi}_2 u_1(p)|$ and the θ-function controls the boundary below which the data in channel L2 are unsuitable for processing (as a rule, $p_2 > p_1$). For $p \in [p_1, p_2]$, the bending angles in channel L2 $\varepsilon_2(p)$ were defined as $\varepsilon_1(p) + \Delta\varepsilon(p)$, where $\Delta\varepsilon(p)$ is an estimate of the ionospheric difference $\varepsilon_2(p) - \varepsilon_1(p)$, which is calculated over the interval of impact parameters $[p_1, p_1 + 1\ \text{km}]$.

The profiles of bending angles $\varepsilon_{1,2}(p)$ contain the contribution of the ionosphere. Since the ionospheric contribution is inversely proportional to the frequency squared, in the context of the linear approximation, one can eliminate the ionospheric contribution and calculate the component of the bending angle $\varepsilon(p)$ related to the neutral atmosphere [38–41]. At heights above 50 km, the ionospheric component of the bending angle becomes substantially greater than the neutral component. As a result, it is possible to estimate the residual error of the ionospheric correction $\delta\varepsilon_I(p)$ in the profile of the bending angle $\varepsilon(p)$ [40].

4.3. Estimation of the Errors of Bending Angles

The errors of $\varepsilon(p)$ in the lower troposphere are estimated from analysis of the local spectra of the transformed wave field $\hat{\Phi}_2 u_1(p) = A'(p)\exp(ik\Psi'(p))$. For this purpose, the eikonal $\overline{\Psi}'(p)$ smoothed with a 0.25-km window and moving spectra are calculated similarly to (9):

$$w(p, \xi) = \int_{p-\Delta p/2}^{p+\Delta p/2} \cos\frac{\pi(p' - p)}{\Delta p} \frac{\hat{\Phi}_2 u_1(p')}{\exp(ik\overline{\Psi}'(p))} \times \exp(-ik\xi p')dp', \quad (49)$$

where $\Delta p = 1$ km. The spectral peak is, on the average, located near $\xi = 0$. The tropospheric error of the bending angle $\delta\varepsilon_T(p)$ is estimated as the width of the spectrum:

$$\delta\varepsilon_T(p) = \left(\frac{\int|w(p, \xi)|^2\xi^2 d\xi}{\int|w(p, \xi)|^2 d\xi}\right)^{1/2}. \quad (50)$$

The rms error $\delta\varepsilon(p)$ in determining the bending angle was taken equal to $\delta\varepsilon_I(p)$ for heights of the ray $p - r_E > 10$ km and to $\delta\varepsilon_T(p)$ for heights of the ray $p - r_E < 10$ km.

4.4. Inversion and the Estimation of Errors in the Retrieved Temperature

With the use of the Abelian inversion (see (4)), the refractive index $n(r)$ is calculated from the neutral-atmosphere component $\varepsilon(p)$ of the bending angle. The variance of the retrieved refractive index is calculated as

$$\langle\delta n^2(x)\rangle = \iint_x^\infty \frac{\langle\delta\varepsilon(p')\delta\varepsilon(p'')\rangle dp'dp''}{\sqrt{p'^2 - x^2}\sqrt{p''^2 - x^2}}, \quad (51)$$

where the covariance matrix of bending angles, $\langle\delta\varepsilon(p')\delta\varepsilon(p'')\rangle$, is taken equal to $\delta\varepsilon^2(p)$ for $p' = p'' = p$ and, for the other values of p' and p'', it is assumed to be a triangular matrix with a characteristic width of 1 km in accordance with the estimates obtained in [41].

For the error in temperature retrieval, the following expression is obtained from (6):

$$\langle\delta T^2(z)\rangle = \frac{\langle\delta n^2(z)\rangle}{[n(z) - 1]^2}T^2 - 2\frac{z\int_z^\infty g(z')\langle\delta n(z)\delta n(z')\rangle dz'}{R[n(z) - 1]^2}T + \frac{z^2\iint_z^\infty g(z'')g(z')\langle\delta n(z')\delta n(z'')\rangle dz'dz''}{R^2[n(z) - 1]^2}. \quad (52)$$

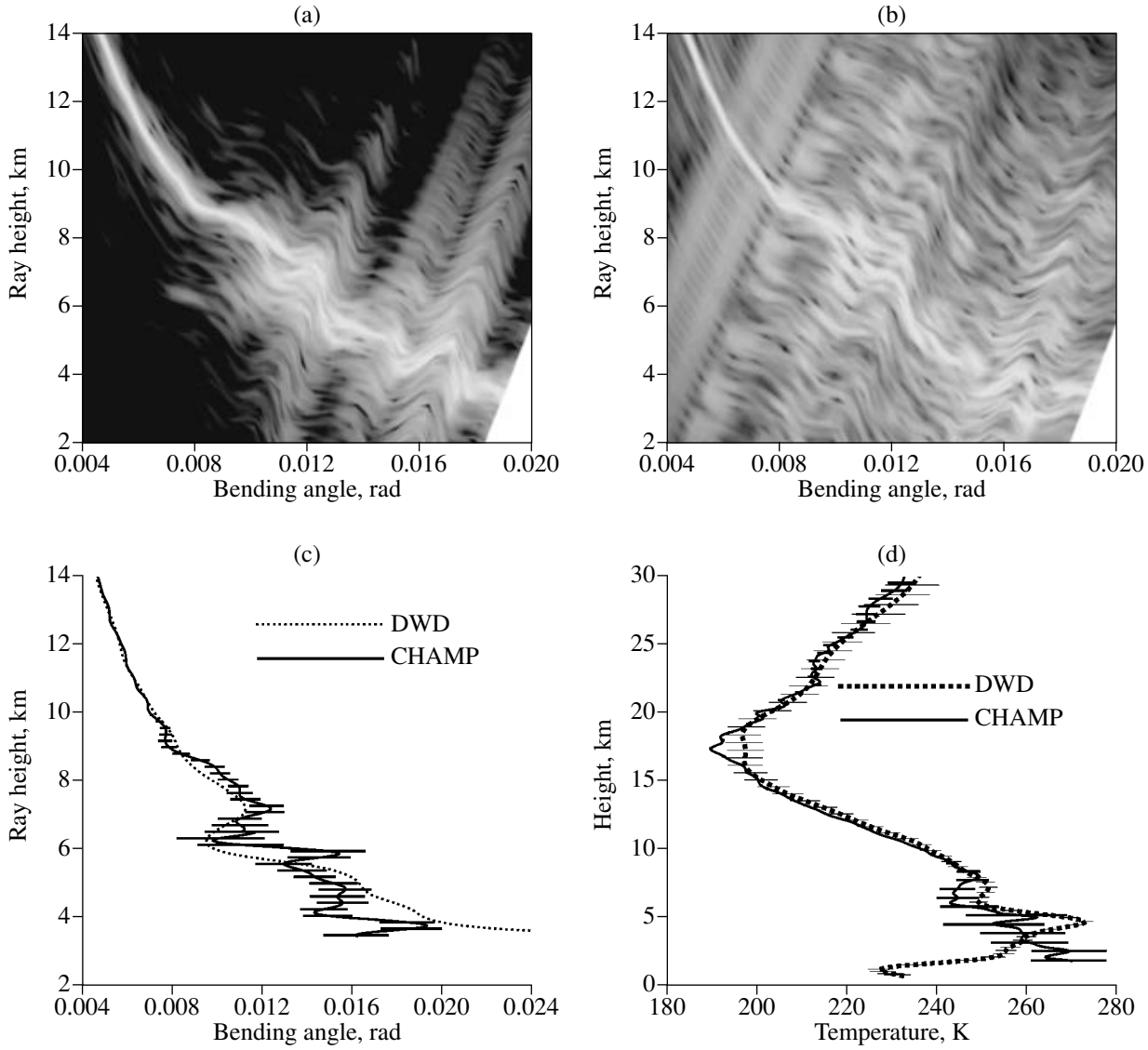

Fig. 4. Occultation event 0041, Jan. 18, 2004; UT = 04:09; 26.0° S, 19.4° E: (a) local spatial spectra for channel L1, (b) the same for channel L2, (c) bending angles calculated for the fields of DWD analyses and from the CHAMP data, and (d) temperature from the data of DWD analyses and CHAMP data.

Assuming that the correlation length of the error $\delta n(z)$ is substantially smaller than the homogeneous-atmosphere height, one can approximately write

$$\sigma_{\text{CHAMP}} \equiv \langle \delta T^2 \rangle^{1/2} = \langle \delta n^2 \rangle^{1/2} \frac{T}{n-1}. \qquad (53)$$

4.5. Examples

Below, examples of processing the data of CHAMP measurements are given. We determine bending angles and temperature profiles and estimate their errors by formulas (50) and (53). The bending angles and temperatures calculated from the global meteorological fields taken from the recent analysis of the German Weather Service (Deutscher WetterDienst—DWD) are also presented. It is significant that the discrepancy between the radio occultation data and the DWD data includes both the errors of the radio occultation data and the errors of analysis. To assess the degree of agreement between the radio occultation data and the DWD analyses, we also present the errors of temperature profiles estimated from the analyses of σ_{DWD}.

Figures 3c and 3d show the bending angles and temperatures retrieved from a CHAMP occultation event and the estimates of their errors. Above 25 km, the errors of temperature retrieval related to the background ionospheric fluctuations start to increase and constitute about 5 K at a height of 30 km. Above 30 km, the value of radio occultation data for dynamic weather forecasting becomes low [40, 41]. Between 25 and

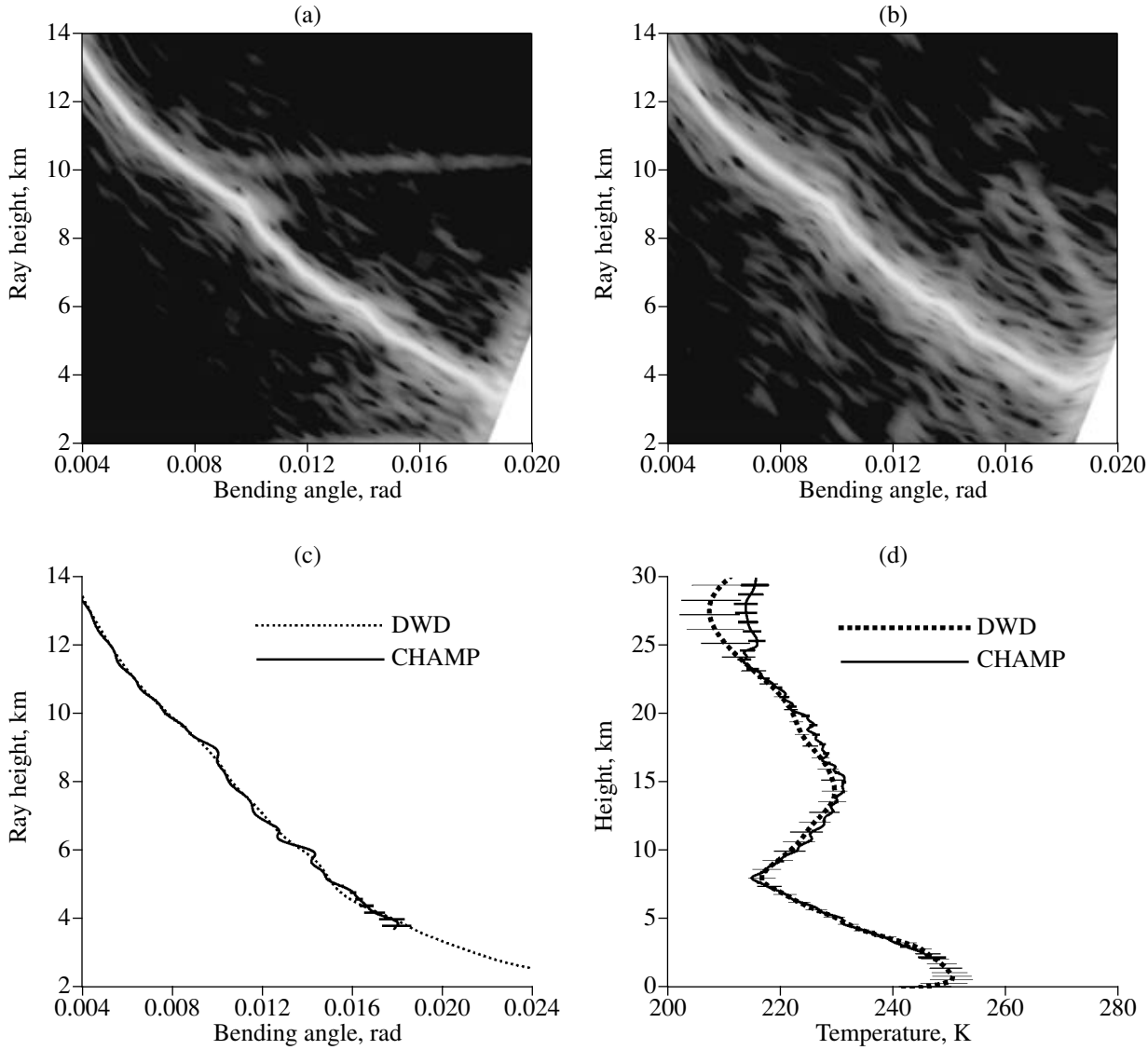

Fig. 5. Occultation event 0097, Jan. 18, 2004; UT = 09:50; 78.8° N, 125.6° W: (a) local spatial spectra for channel L1, (b) the same for channel L2, (c) bending angles calculated for the fields of DWD analyses and from the CHAMP data, and (d) temperature from the data of DWD analyses and CHAMP data.

7 km, the estimated errors in temperature retrieval turn out to be small (basically within 1 K). This is due to the fact that the bending angles in this height range are sufficiently large compared to the background ionospheric fluctuations and the effects of multipath propagation are of little importance for GPS frequencies. Therefore, the accuracy of amplitude and phase measurements turns out to be fairly high. Below 7 km, multipath propagation occurs, a phenomenon which is observed from the nonmonotonic profiles of bending angle obtained from both CHAMP data processing and DWD analyses of meteorological fields. The estimated errors in determining bending angles and temperature increase substantially here.

Figure 4 presents the results of processing the data of another occultation event. In this session, ionospheric fluctuations are weaker than those in the previous example and the estimated error in temperature retrieval amounts to about 3 K at a height of 30 km. The profile of the bending angle is nonmonotonic below 8 km, which is indicative of multipath propagation. The spectra exhibit a high level of noise in channel L2 below 12 km. In multipath regions, the level of noise in channel L2 increases significantly. An increase in the errors of the bending angles in multipath-propagation regions leads to an increase in the errors of temperature retrieval, which amount to about 5–10 K below 7 km.

Figure 5 presents the results of processing the data of a occultation event characterized by a good quality of the signal and a low level of errors. In all the examples presented above, the discrepancy between the

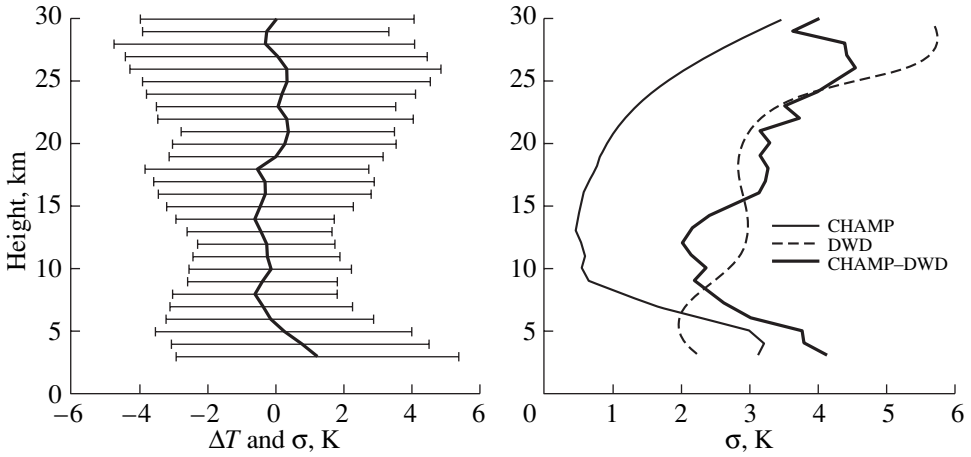

Fig. 6. Statistical comparison of the temperatures retrieved from the CHAMP data with DWD analyses of Jan. 18, 2004: mean deviation and rms spread (on the left). The mean estimate of errors in the CHAMP data, the mean estimate of errors in the DWD data, and the rms deviation of CHAMP – DWD (on the right).

CHAMP and DWD data is consistent with the estimated errors and is no greater than

$$2(\sigma^2_{\mathrm{CHAMP}} + \sigma^2_{\mathrm{DWD}})^{1/2}.$$

Statistical comparison was also made between radio occultation data and DWD data on the basis of 90 occultation events conducted during January 18, 2004 (Fig. 6). A systematic difference between the CHAMP and DWD data is no greater than 0.5 K at heights above 5 km. The rms data spread is 2–4 K. The largest systematic discrepancy is observed in the lower 5-km layer, where it reaches 4 K according to the data presented in [7, 37]. Here, statistical comparison is made only for heights greater than 3 km, where the systematic difference does not exceed 1 K. Below 3 km, the amount of radio-occultation data decreases substantially, thus making the results of statistical analysis less reliable. As was noted above, the increase in systematic errors in the lower troposphere is due to an unstable operation of the receiver in the regions of multipath propagation, where the signal can be lost. A more detailed statistical analysis was carried out in [7, 37] on the basis of a longer series of observations and the data of the European Centre of Medium-Range Weather Forecasts.

We also compared the discrepancies between the CHAMP and DWD data with independent estimates of the errors in the CHAMP and DWD data. The errors in the CHAMP data were estimated using the method described in this paper. The errors in the DWD data were estimated from a comparison of DWD numerical forecasts with the data of real measurements. The estimated errors in the CHAMP data σ_{CHAMP} and DWD data σ_{DWD} and the rms difference CHAMP – DWD are plotted in Fig. 6 on the right. All data presented are averaged over 90 occultation events conducted during January 18, 2004. The plots demonstrate that the estimated errors in the CHAMP and DWD data are in good agreement with the discrepancy between these data. In the height ranges 8–15 km and above 24 km, the estimated errors in DWD analyses seem to be somewhat overstated.

5. CONCLUSIONS

Methods for interpreting the data of satellite radio-occultation remote sensing of the Earth's atmosphere with the aid of GPS signals were discussed. The methods include (1) the filtering of noise and inferior data in channel L2 on the basis of analysis of the local spatial spectra of the measured wave field, (2) the determination of bending angles by the canonical transform method, (3) the estimation of the errors in bending angles from analysis of the local spatial spectra of the transformed wave field, (4) ionospheric correction combined with statistical regularization, (5) the Abelian inversion of the profiles of bending angle for obtaining the profiles of refractive index, and (6) the retrieval of temperature profiles in the hydrostatic approximation. It is significant that the errors can be estimated without using a priori information. At large heights, the background ionospheric fluctuations predominate in the signal. This phenomenon makes it possible to estimate the errors in bending angles above 8–10 km, where the main source of errors is ionospheric fluctuations. The errors in determining the bending angles in the troposphere at heights below 8–10 km are related mainly to multipath propagation. These errors are estimated from the width of the local spectra of the transformed wave field. The errors related to multipath propagation in the troposphere turn out to be rather significant. This result implies that the existing receiver needs modification. On the other hand, this problem is not fundamental and has a purely engineering character. In the opinion of most specialists in the field of radio-occultation sounding, this problem should be

solved by successively employing open-loop facilities in the signal tracking circuit. Statistical comparison was made between the CHAMP data and the data of analyses of the German Weather Service (DWD). Such a comparison has shown that the estimated errors in the CHAMP and DWD data are in good agreement with the rms discrepancies between the CHAMP and DWD data. The ultimate goal of developing the methods of data processing and estimating the errors in retrieved temperature profiles is the use of these methods in the system of a direct variational assimilation of radio-occultation data into an atmospheric global-circulation model. Work on incorporating the algorithms described in this paper into the data assimilation system of the German Weather Service is being carried out at the present time.

ACKNOWLEDGMENTS

The authors are grateful to A.S. Gurvich, V.I. Klyatskin, I.G. Yakushkin, S.V. Sokolovskiy (Institute of Atmospheric Physics, Russian Academy of Sciences), Yu.A. Kravtsov (Institute for Space Research, Russian Academy of Sciences), and A.S. Jensen (Danish Meteorological Institute, Copenhagen) for useful discussions of the issues discussed in the paper.

This study was supported by the Russian Foundation for Basic Research, project no. 03-05-64366.

REFERENCES

1. E. R. Kursinski, G. A. Hajj, S. S. Leroy, and B. Herman, "The GPS Radio Occultation Technique," Terr. Atmos. Ocean. Sci. **11** (1), 53–114 (2000).
2. A. S. Gurvich and T. G. Krasil'nikova, "Navigation Satellites for Radio Sounding of the Earth's Atmosphere," Issled. Zemli Kosmosa **7**, 1124–1131 (1987).
3. E. R. Kursinski, G. A. Hajj, W. I. Bertiger, *et al.*, "Initial Results of Radio Occultation Observation of Earth's Atmosphere Using the Global Positioning System," Science **271**, 1107–1110 (1996).
4. R. Ware, M. Exner, D. Feng, *et al.*, "GPS Sounding of the Atmosphere from Low Earth Orbit: Preliminary Results," Bull. Am. Meteorol. Soc. **77** (1), 19–40 (1996).
5. C. Rocken, R. Anthes, M. Exner, *et al.*, "Analysis and Validation of GPS/MET Data in the Neutral Atmosphere," J. Geophys. Res. D **102**, 29849–29866 (1997).
6. K. Steiner, G. Kirchengast, and H. P. Ladreiter, "Inversion, Error Analysis, and Validation of GPS/MET Data," Ann. Geophys. **17**, 122–138 (1999).
7. M. E. Gorbunov and L. Kornblueh, "Analysis and Validation of GPS/MET Radio Occultation Data," J. Geophys. Res. D **106**, 169 (2001).
8. J. Wickert, C. Reigber, G. Beyerle, *et al.*, "Atmosphere Sounding by GPS Radio Occultation: First Results from CHAMP," Geophys. Rev. Lett. **28**, 3263–3266 (2001).
9. J. R. Eyre, "Assimilation of Radio Occultation Measurements into a Numerical Weather Prediction System," Technical Memorandum No. 199 (European Center for Medium-Range Weather Forecast, 1994).
10. X. Zou, Y.-H. Kuo, and Y.-R. Guo, "Assimilation of Atmospheric Radio Refractivity Using a Nonhydrostatic Adjoint Model," Mon. Weather Rev. **123**, 2229–2249 (1995).
11. H. Liu and X. Zou, "Improvements to a GPS Radio Occultation Ray-Tracing Model and Their Impacts on Assimilation of Bending Angle," J. Geophys. Res. D **108**, 4548 (2003); doi: 10.1029/2002JD003160.
12. M. E. Gorbunov and L. Kornblueh, "Principles of Variational Assimilation of GNSS Radio Occultation Data," Report No. 350 (Max Planck Institute for Meteorology, Hamburg, 2003).
13. V. V. Vorob'ev and T. G. Krasil'nikova, "Estimating the Accuracy of Retrieving the Atmospheric Refractive Index from Measurements of the Doppler Shift at the NAVSTAR Frequencies," Izv. Akad. Nauk SSSR, Fiz. Atmos. Okeana **29**, 626–632 (1993).
14. A. G. Pavel'ev, "On a Possible Radio Holographic Study of Radio Fields near the Radio-Shadow Zone on Satellite–Satellite Paths," Radiotekh. Elektron. (Moscow) **43** (8), 875–879 (1998).
15. K. Igarashi, A. Pavelyev, K. Hocke, *et al.*, "Radio Holographic Principle for Observing Natural Processes in the Atmosphere and Retrieving Meteorological Parameters from Radio Occultation Data," Earth, Planets, Space **52**, 893–899 (2000).
16. A. I. Zakharov, A. G. Pavel'ev, V. P. Sinilo, *et al.*, "Development of Satellite Methods of Radio Holographic Observations of the Earth's Surface and Atmosphere," Kosm. Issled. **41**, 610–615 (2004).
17. M. E. Gorbunov, "Canonical Transform Method for Processing GPS Radio Occultation Data in Lower Troposphere," Radio Sci. **37**, 9-1–9-10 (2002); doi: 10.1029/2000RS002592.
18. A. S. Jensen, M. S. Lohmann, H.-H. Benzon, and A. S. Nielsen, "Full Spectrum Inversion of Radio Occultation Signals," Radio Sci. **38**, 6-1–6-15 (2003); doi: 10.1029/2002RS002763.
19. M. E. Gorbunov and K. B. Lauritsen, "Canonical Transform Methods for Radio Occultation Data," Scientific Report No. 02–10 (Danish Meteorological Institute, Copenhagen, 2002); http://www.dmi.dk/dmi/Sr02-10.pdf.
20. A. S. Jensen, M. S. Lohmann, A. S. Nielsen, and H.-H. Benzon, "Geometrical Optics Phase Matching of Radio Occultation Signals," Radio Sci. **39**, RS3009 (2004); doi: 10.1029/2003RS002899.
21. S. V. Sokolovskiy, "Modeling and Inverting Radio Occultation Signals in the Moist Troposphere," Radio Sci. **36**, 441–458 (2001).
22. S. V. Sokolovskiy, "Tracking Tropospheric Radio Occultation Signals from Low Earth Orbit," Radio Sci. **36**, 483–498 (2001).
23. G. Beyerle, M. E. Gorbunov, and C. O. Ao, "Simulation Studies of GPS Radio Occultation Measurements," Radio Sci. **38**, 1084 (2003); doi: 10.1029/2002RS002800.
24. O. I. Yakovlev, *Space Radiophysics* (Nauchnaya kniga, Moscow, 1998) [in Russian].
25. A. S. Gurvich and S. V. Sokolovskii, "On Retrieving the Pressure Field by Remote Refractometry from Space," Izv. Akad. Nauk SSSR, Fiz. Atmos. Okeana **21**, 12–21 (1985).

26. R. A. Phinney and D. L. Anderson, "On the Radio Occultation Method for Studying Planetary Atmospheres," J. Geophys. Res. **73**, 1819–1827 (1968).

27. G. F. Lindal, J. R. Lyons, D. N. Sweetnam, *et al.*, "The Atmosphere of Uranus: Results of Radio Occultation Measurements with Voyager," J. Geophys. Res. A **92**, 14987–15001 (1987).

28. M. E. Gorbunov, A. S. Gurvich, and L. Kornblueh, "Comparative Analysis of Radioholographic Methods of Processing Radio Occultation Data," Radio Sci. **35**, 1025–1034 (2000).

29. M. E. Gorbunov, "Radio-Holographic Analysis of Radio Occultation Data in Multipath Zones," Radio Sci. **37**, 14-1–14-9 (2002); doi: 10.1029/2000RS002577.

30. M. E. Gorbunov, "Radio-Holographic Analysis of Microlab-1 Radio Occultation Data in the Lower Troposphere," J. Geophys. Res. D **107**, 7-1–7-10 (2002); doi: 10.1029/2001JD000889.

31. Yu. A. Kravtsov and Yu. I. Orlov, *Geometrical Optics of Inhomogeneous Media* (Nauka, Moscow, 1980; Springer, Berlin, 1990).

32. A. S. Mishchenko, B. Yu. Sternin, and V. E. Shatalov, *Lagrangian Manifolds and the Canonical Operator Method* (Nauka, Moscow, 1978) [in Russian].

33. V. I. Arnold, *Mathematical Methods of Classical Mechanics* (Nauka, Moscow, 1978; Springer, New York, 1989).

34. M. E. Gorbunov and K. B. Lauritsen, "Analysis of Wave Fields by Fourier Integral Operators and Its Application for Radio Occultations," Radio Sci. **39**, RS4010 (2004); doi: 10.1029/2003RS002971.

35. A. G. Pavel'ev and A. I. Kucheryavenkov, "Theory of Refraction Attenuation of Radio Waves in Planetary Atmospheres," Radiotekh. Elektron. (Moscow) **23**, 1345–1351 (1978).

36. C. O. Ao, T. K. Meehan, G. A. Hajj, *et al.*, "Lower-Troposphere Refractivity Bias in GPS Occultation Retrievals," J. Geophys. Res. D **108**, 4577 (2003); doi: 10.1029/2002JD003216.

37. M. E. Gorbunov and L. Kornblueh, "Analysis and Validation of Challenging Minisatellite Payload (CHAMP) Radio Occultation Data," J. Geophys. Res. D **108**, 4584 (2003); doi: 10.1029/2002JD003175.

38. S. Sokolovskiy and D. Hunt, "Statistical Optimization Approach for GPS/MET Data Inversions" (URSI GPS/MET Workshop, Tucson, AZ, 1996).

39. S. Syndergaard, "On the Ionospheric Calibration in GPS Radio Occultation Measurements," Radio Sci. **35**, 865–883 (2000).

40. M. E. Gorbunov, "Ionospheric Correction and Statistical Optimization of Radio Occultation Data," Radio Sci. **37**, 17-1–17-9 (2002); doi: 10.1029/2000RS002370.

41. V. V. Vorob'ev and V. Kan, "Background Fluctuations in the Ionosphere during GPS–Microlab-1 Radio-Occultation Experiment," Izv. Vyssh. Uchebn. Zaved., Radiofizika **42**, 511–523 (1999).